Electronic Supplementary Information

In-situ growth of metallic 1T-WS_2 nanoislands on single-walled carbon nanotube films for improved electrochemical performance

Qun He[a+], Weiyu Xu[a+], Shuangming Chen[a], Daobin Liu[a], Muhammad Habib[a], Qin Liu[a], Changda Wang[a], Yasir A. Haleem[a], Ting Xiang[a], Chuanqiang Wu[a], Adnan Khalil[a], Qi Fang[a], Zhiqiang Niu[b] and Li Song[a,*]

[a] *National Synchrotron Radiation Laboratory, CAS Center for Excellence in Nanoscience, University of Science and Technology of China, Hefei, Anhui 230029, China*

[b] *Key Laboratory of Advanced Energy Materials Chemistry (Ministry of Education), College of Chemistry, Collaborative Innovation Center of Chemical Science and Engineering, Tianjin, China*

[+]Equally contributed to this work

***** Corresponding Auther: song2012@ustc.edu.cn

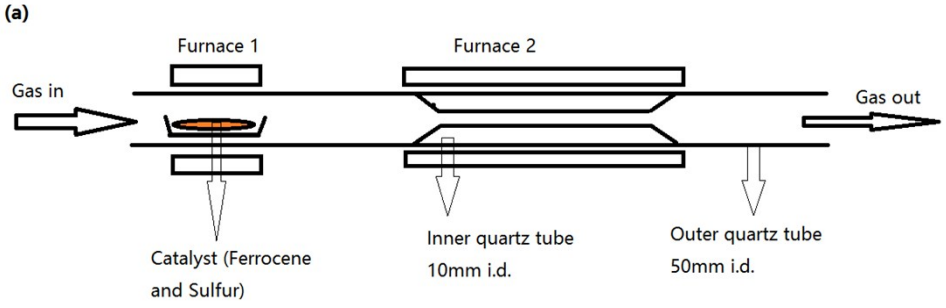

Scheme S1: the configuration of synthesis set-up for SWCNT preparation via a floating chemical vapor deposition method.

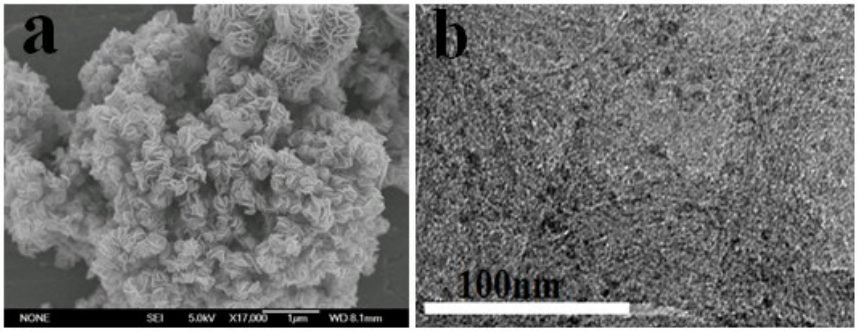

Fig. S1: (a) SEM image of pure 1T-WS_2 and (b) low-magnification TEM image of 1T-WS_2@SWCNT hybrids.

The SEM of pure 1T-WS_2 shows the severe agglomeration. For this, fewer active sites will be exposed to improve its intrinsic HER performance and evidently worse than chemically exfoliated samples[S2,S7], which is consistent with our result showed in Figure 3a. To solve the adverse phenomena, we here use the high-conductive SWCNT as a substrate. Obviously, no glomeration was seen and the thinner and smaller nanoislands dispersed on the surface of SWCNT randomly. Due to this, enhanced electrochemical behavior was achieved in our work.

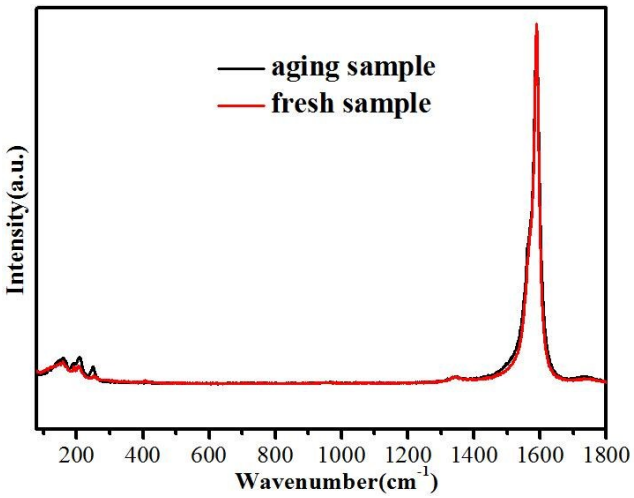

Fig. S2: The Raman spectra of 1T-WS_2@SWCNT hybrids from fresh one (red line) and ten-months aging one (black line), respectively. The Raman spectra of fresh and aging 1T-WS_2@SWCNT hybrids above showed the similar result, which to some extent indicates the phase stability and the unchanged components.

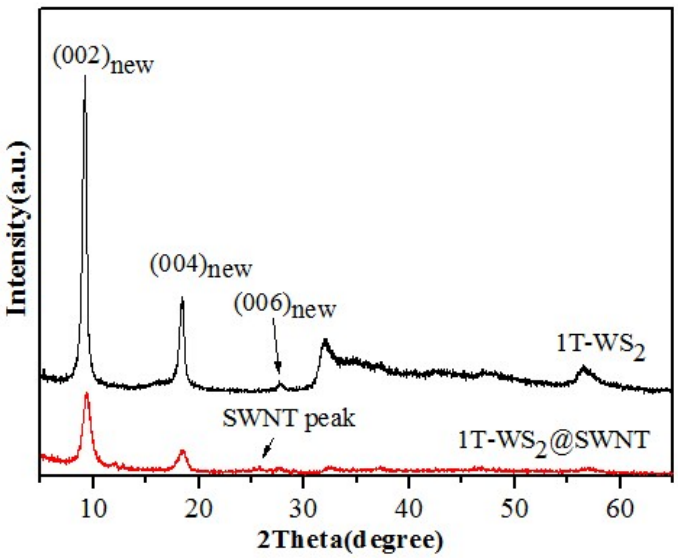

Fig. S3: XRD patterns of 1T-WS_2 (black curve) and 1T-WS_2@SWCNT (red curve).

The X-ray diffraction (XRD) was utilized to certify the structure and composition. it can be seen that the (002) $_{new}$ peak of the 1T-WS_2 samples was found at 9.3°, as well as the corresponding junior diffraction peak (004) $_{new}$ and (006) $_{new}$ peaks were observed in the range of 16°–30°, and with Bragg formula the calculated S-W-S interlayer spacing is 9.4Å for 1T-WS_2 samples, which is agreed with the result we reported before[S1], and the relatively intense (00*l*) reflections reflect the dominant intercalation trait[S2]. To ensure the successful formation of 1T-WS_2 on SWCNT, the XRD for 1T-WS_2@SWCNT hybrid was also tested, and the main occurred peaks was corresponded with the only 1T-WS_2 and a weak diffraction peak of SWCNT (at ~26.5°) existed as well, which to some extent evidenced that the 1T-WS_2@SWCNT hybrid is successfully formed in our work.

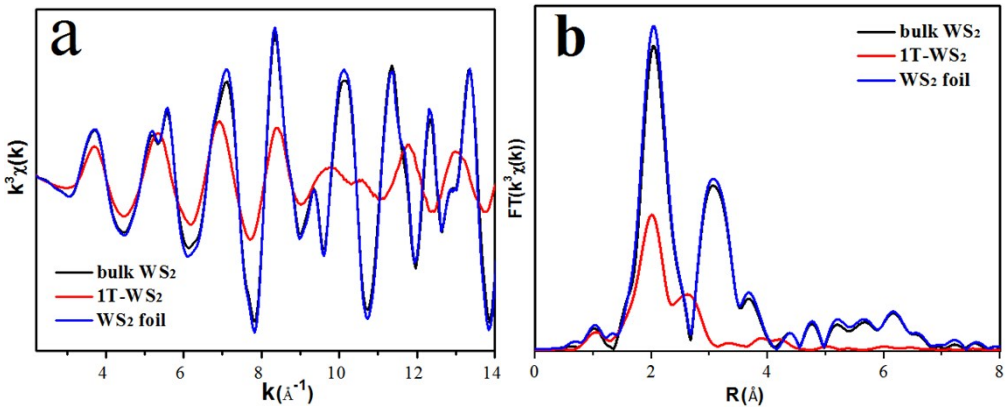

Fig. S4: (a) W L_3-edge oscillation functions $\kappa^3\chi(k)$ and (b) the corresponding FT analysis reveals the shortening of W-W bond length in the new 1T-WS_2 contrast with bulk of sample and foil.

The XAFS result of W L_3-edges in 1T-WS_2 in contrast with bulk WS_2 sample showed in Figure S2a, in which the

oscillation curve of 1T-WS_2 at the k range of 2.2-14.0 $Å^{-1}$ is notably different from that of bulk material, suggesting a major transforming in the local atomic arrangements among these two samples. Additionally, the more direct observation of altered atomic arrangements can be seen from the Fourier transform (FT) curves in the real space. Figure S2b reveals that the FT curves of bulk material possesses two main peaks at about 2.41 Å and 3.17 Å, corresponding to the nearest W-S and W-W bond, respectively. Differently, the W-W bond-corresponded peak of 1T-WS_2 and 1T-WS_2@SWCNT hybrid has the weaker intensity and reduced bond length coordinate ~2.75 Å, in comparison to the bulk one and foil. These observations are close to our HAADF results which we reported previously[S1].

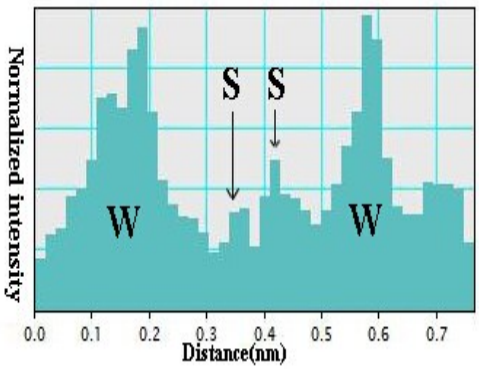

Fig. S5: The intensity profile along the red line in Figure 1c. It can be seen that the intense contrast between W and S sites exists, contributed to the reason that S atoms in 1T-WS_2 are uniformly dispersed around W sites.

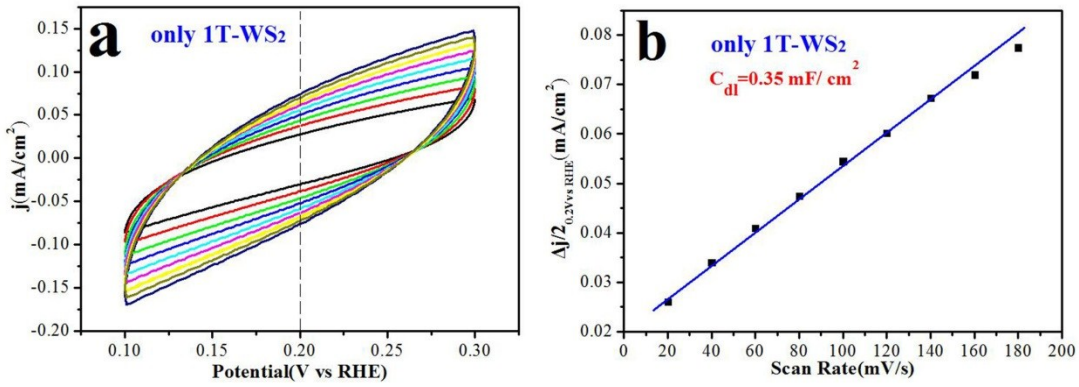

Fig. S6: (a) Cyclic voltammograms measurement of 1T-WS_2@SWCNT hybrid in the region of 0.10-0.30V vs.RHE, in which no faradic process were seen to obtain the capacitive current. (b) The calculated EDLC from (a) at an overpotential of +0.20V vs. RHE. The calculated EDLC value from CV like that of 1T-WS_2@SWCNT hybrid is very small (~0.35mF/cm2), which possibly due to the severe aggregation inducing less exposed surface.

Table S1: Structural parameters for W and S atoms in foil, bulk 2H-WS_2 and 1T-WS_2 fitted from EXAFS data, respectively. The structure of 1T-WS_2 is strongly distorted compared to bulk 2H-WS_2.

Sample	Path	R(Å)	N	$\sigma^2(10^{-3}$ Å$^2)$
Foil	W-S	2.41	6	3.6
	W-W	3.17	6	3.8
Bulk WS_2	W-S	2.41	5.8	3.9
	W-W	3.17	6	4.2
1T-WS_2	W-S	2.41	4.3	8.3
	W-W	2.75	1.7	5.1

R, bond distance; N, coordination number; σ2, Debye-Waller factor; Error bounds (accuracies) were estimated as R, ±1%, N, ±5%; σ2, ±1%.

Table S2: The different EDLC values in several recent literature.

Reference	Method	State	EDLC
This work	In-situ solvothermal synthesis	Nanosheets (NSs)	226mF/cm^2
Ref. S2	Solvothermal method and plasma-assisted CVD	NSs	7.96 mF/cm^2
Ref. S3	hydrothermal method	NSs	21 mF/cm^2
Ref. S4	High temperature solid reaction and Lithium intercalation	Nanotubes (NTs) Nanoribbons-Li(NRs-Li)	1.27 mF/cm^2 6.03 mF/cm^2
Ref. S5	Hydrothermal method	NSs	5.8 mF/cm^2
Ref. S6	Chemically exfoliated from WS_2 nanostructures synthesized by CVD method	As-grown NSs 20min microwave NSs	2.7 mF/cm^2 47.8 mF/cm^2
Ref. S7	Low-temperature wet chemical method	Amorphous layered MoSx	5.11 mF/cm^2
Ref. S8	Chemical exfoliation	As-grown NSs n-BuLi treated NSs	4.6μF/cm^2 75μF/cm^2

Table S3: The HER performance for various MS_2 (M=W or Mo)-based materials.

Reference	Method	State	Overpotentials (mV)	Tafel Slope (mV/dec)	Stability	Potential (mV) at j=10mA/cm^2
This work	In-situ solvothermal synthesis	Nanosheets (NSs)	25-30	57	Stable	108
Ref. S2	Solvothermal method and plasma-assisted CVD	NSs	~180	41.3	Stable	~210
Ref. S9	Solvothermal method	NSs	~115	41	Stable	~150
Ref. S3	Hydrothermal method	NSs	~125	47	Stable	~180
Ref. S11	Reaction of WO_3 with S at 830℃ by CVD	NSs	~110	~100	Stable	~320
Ref. S12	A lithium-based electrochemical anodization and low temperature sulfurization	NSs	30	61	Stable	136
Ref. S5	Hydrothermal method	NSs	~190	73	NA	229
Ref. S4	High temperature solid reaction and Lithium intercalation	Nanoribbons, (NRs) NRs-Li	~140 ~100	77 (S NRs) 68 (S NRs-Li)	Stable	203 173
Ref. S13	Solvothermal method	NSs	~170	40.82	Stable	~215
Ref. S6	Chemically exfoliated from WS_2 nanostructures synthesized by CVD method	NSs	75	70	NA	142
Ref. S14	Solution synthesis with S, WCl_6, and several organic matters, followed by annealing at 500℃	Nanoflkes (NFs)	100	48	Stable	~280
Ref. S15	Lithium intercalation and exfoliation from bulk WS_2	NSs	80-100(1T) 150-200（2H）	~60（1T） ~115（2H）	Stable	~260
Ref. S16	Solvothermal method	NSs	140	44.6	Stable	185
Ref. S8	Chemical exfoliation	NSs	~130	43	Stable	187
Ref. S17	Hydrothermal synthesis in the presence of RGO nanosheets, then vacuum annealing at 300℃	NSs	~150	58	NA	~260
Ref. S18	Mechanical activation	NSs-ball-milling NSs	60	72	Stable	150

			120	138		NA

Reference:

S1 Q. Liu, X. Li, Z. Xiao, Y. Zhou. H. Chen, K. Adnan, T. Xiang, J. Xu, W. Chu, X. Wu, J. Yang, C. Wang, Y. Xiong, C. Jin, M. A. Pulickel and L. Song, *Adv. Mater.*, 2015, 27, 4837-4844.

S2 Y. Wang, B. Chen, D. Seo, Z. Han. J. Wong, K. Ostrikov, H. Zhang and H. Yang, *NPG Asia Mater*, 2016, 8, e268.

S3 Z. Xiang, Z. Zhang, X. Xu, Q. Zhang and C. Yuan, *Carbon*, 2016, 98, 84-89.

S4 Y. Yang, H. Fei, G. Ruan, Y. Li and M. James, *Adv. Funct. Mater*, 2015, 25, 6077-6083.

S5 A. S. Tofik, F. Wang, Z. Cheng, X. Zhan, Z. Wang, K. Liu, S. Muhammad, L. Sun and J. He, *Nanoscale*, 2015, 7, 14760-14765.

S6 M. A. Lukowski, A. S. Daniel, C. R. English, F. Meng, A. Forticaux, R. J. Hamers and S. Jin, *Energy Environ. Sci.*, 2014, 7(8): 2608-2613.

S7 D. Li, U. Maiti, J. Lim, D. Choi, W. Lee, Y. Oh, G. Lee and S. Kim, *Nano Lett*, 2014, 14, 1228−1233.

S8 A. L. Mark, S. D. Andrew, F. Meng, F. Audrey, L. Li and S. Jin, *J. Am. Chem. Soc.* 2013, 135, 10274−10277.

S9 D. Liu, W. Xu, Q. Liu, Q. He, A. Yasir, C. Wang, T. Xiang, C. Zou, W. Chu, J. Zhong, Z. Niu and L. Song, *Nano Res*, 2016, 9, 2079−2087.

S10 S. Dou, J. Wu, L. Tao, A. Shen, J. Huo and S. Wang, *Nanotech*, 2016, 27, 045402.

S11 Y. Zhang, J. Shi, G. Han, M. Li, Q. Ji, D. Ma, Y. Zhang, C. Li, X. Lang, Y. Zhang and Z. Liu, *Nano Res*, 2015, 8, 2881-2890.

S12 Y. Yang, H. Fei, G. Ruan, Y. Li and M. James, *Adv. Funct. Mater*,2015, 25, 6199-6204.

S13 Y. Cai, X. Yang, T. Liang, L. Dai, L. Ma, G. Huang, W. Chen, H. Chen, H. Su and M. Xu, *Nanotech*, 2014, 25, 465401.

S14 L. Cheng, W. Huang, Q. Gong, C. Liu, Z. Liu, Y. Li and H. Dai, *Angew.Chew.Int.Ed*., 2014, 53, 7860–7863.

S15 V. Damien, Y. Hisato, J. Li, S. Rafael, C. B. A. Diego, F. Takeshi, M. Chen, A. Tewodros, B. S. Vivek, E. Goki, and C. Manish, *Nat. mater.*, 2013. 12,850-855.

S16 Y. Yan, X. Ge, Z. Liu, J. Wang, J. Lee and X. Wang, *Nanoscale* , 2013, 5, 7768-7771.

S17 Y. Jieun, V. Damien, J. A. Seong, D. Kang, Y. K. Ah, C. Manish and S. S. Hyeon, *Angew. Chem. Int. Ed.*, 2013, 52, 1-5.

S18 Z. Wu, B. Fang, B. Arman, S. Aokui, P. W. David, D. Wang, *Appl. Catal. B: Environ*, 2012, 125, 59-66.